Available online at www.sciencedirect.com

SciVerse ScienceDirect

Ceramics International 38 (2012) 5145–5149

CERAMICS INTERNATIONAL

www.elsevier.com/locate/ceramint

SnO_2 nanorods grown on graphite as a high-capacity anode material for lithium ion batteries

Hongdong Liu, Jiamu Huang *, Xinlu Li *, Jia Liu, Yuxin Zhang

School of Materials Science and Engineering, Chongqing University, Chongqing 400045, China

Received 15 December 2011; received in revised form 4 March 2012; accepted 5 March 2012
Available online 14 March 2012

Abstract

A novel architecture of SnO_2 nanorods grown on graphite has been synthesized by a simple hydrothermal method for lithium ion battery. The as-prepared products were characterized by XRD, FTIR, N_2 adsorption/desorption, FESEM and TEM. The electrochemical performances of SnO_2/graphite composite were measured by cyclic voltammetry, galvanostatic charge/discharge cycling and electrochemical impedance spectroscopy. The results show that the SnO_2/graphite composite maintains high lithium storage capacity and good cycling stability, indicating its promising potential as a novel anode material for high-performance lithium ion batteries.

Keywords: SnO_2 nanorods; Graphite; Lithium ion batteries

1. Introduction

Lithium ion batteries have rapidly dominated the power-source market for portable electronic devices, power tools, and electric vehicles due to their high energy density and excellent cycle life [1]. Graphite based materials are still used as anodes for lithium ion batteries, although the theoretical capacity of 372 mAh g^{-1} is not sufficient [2]; therefore, there is an intensive research effort to identify higher capacity anode materials. So far, various metal oxides [3–8], polymers [2], carbon materials [9] and their composites [10–13] have been exploited as the anode materials of lithium ion batteries. Among them, SnO_2-based materials have attracted great interest as promising substitutes for the commercial graphite anodes because of their low cost, safety, and high theoretical lithium storage capacity (about 782 mAh g^{-1}). However, its large volume expansion/contraction and severe particle aggregation associated with the Li^+ insertion and extraction process lead to pulverization and loss of interparticle contact, consequently, result in a large irreversible capacity loss and poor cycling stability [14–16]. To solve these issues, we used a hydrothermal method to directly grow SnO_2 nanorods on graphite substrate. The as-prepared SnO_2/graphite composite exhibits an enhanced lithium storage capacity and good cyclic performance as anode material in lithium ion batteries.

2. Experimental

2.1. Preparation and characterization

0.1 g natural flake graphite was dispersed in 40 mL of deionized water. Then, 1.05 g of $SnCl_4.5H_2O$ and 1.40 g of NaOH were added into the above suspension. After stirring for 20 min, the mixture was transferred into a PTFE-lined autoclave. The autoclave was sealed and kept at 200 °C for 16 h. The system was then cooled naturally to room temperature. The products were washed with deionized water and ethanol several times, and then dried at 70 °C. The bare SnO_2 was synthesized under the same condition without the addition of graphite for comparison.

X-ray diffraction (XRD) patterns were obtained from DMAX-2500PC using Cu/Ka radiation (λ = 1.5406 Å). Fourier transform infrared spectroscopy (FTIR) spectra were recorded on a GX spectrometer. Brunauer–Emmet–Teller (BET) specific surface area was determined from N_2 adsorption/desorption using automatic specific surface area measuring equipment

* Corresponding authors. Tel.: +86 23 65127306; fax: +86 23 65127306.
E-mail addresses: huangjiamu@cqu.edu.cn (J. Huang), lixinlu@cqu.edu.cn (X. Li).

0272-8842/$36.00
doi:10.1016/j.ceramint.2012.03.019

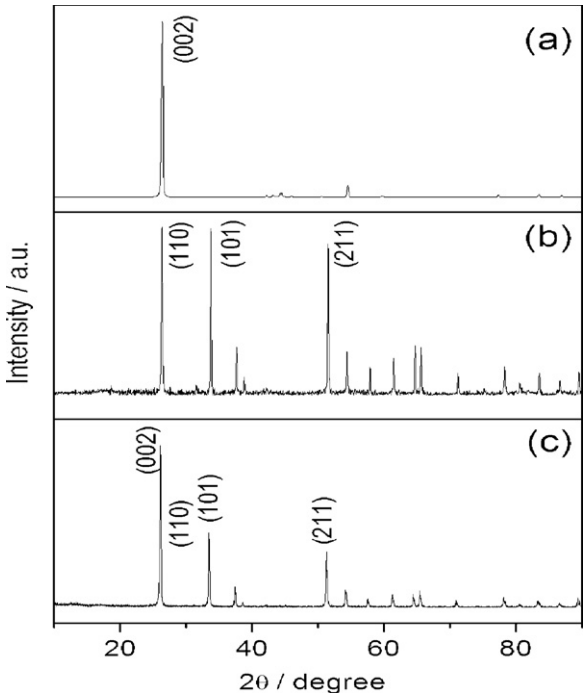

Fig. 1. XRD patterns of (a) graphite, (b) bare SnO_2, (c) SnO_2/graphite composite.

(ASAP 2020M). The structure and morphology of the products were observed by field emission scanning electron microscope (FESEM, NOVA 400) and transmission electron microscope (TEM, LIBRA 200FE).

2.2. Electrochemical measurements

The electrochemical measurements were carried out in coin cells with a Li foil as the counter electrode. The working electrode was prepared by mixing active material (80 wt.%), carbon black (10 wt.%) and polyvinylidone difluoride (PVDF) (10 wt.%) in N-methyl-2-pyrrolidone (NMP) to form a slurry. 1 M $LiPF_6$ in the volume ratio of 1:1 ethyl methyl carbon (EMC)/dimethyl carbonate (DMC) as electrolyte. The cells were galvanostatically charge–discharged in the voltage range 0–3.0 V vs. Li/Li+ at the current densities of 50 mA g^{-1}, 100 mA g^{-1} and 500 mA g^{-1} via a Battery Testing System (Ningbo baite testing equipment Co., China). Cyclic voltammetry (CV) curves were collected at 0.2 mV s^{-1} within the range of 0–3.0 V and electrochemical impedance spectroscopy (EIS) was performed from 0.1 Hz to100 kHz frequency range using Solartron (1260 8w).

3. Results and discussion

The XRD patterns of natural flake graphite, bare SnO_2 and SnO_2/graphite composite are shown in Fig. 1. The sharp peak at around $2\theta = 26.4^\circ$ corresponds to the (0 0 2) reflection of graphite as can be seen from Fig. 1a. Fig. 1b shows the major diffraction peaks are well indexed with the tetragonal rutile phase of SnO_2 which is confirmed by a comparison with standard values (JCPDS 41-1445). Fig. 1c presents the similar phase with that of bare SnO_2 and the (1 1 0) reflection of SnO_2 is overlapped by the (0 0 2) reflection of graphite.

The natural flake graphite powers were obtained from a commercial source. These samples have average dimensions of 30 μm in the direction parallel to the basal plane. It can be seen from Fig. 2a that the surface of graphite is smooth. Fig. 2b presents the SnO_2 nanorods are rectangular in shape and are densely distributed throughout the graphite surface. It is a typical nanorod in Fig. 2c that the length is approximately 1050 nm and the width is around 100 nm. The growth of SnO_2 nanorods occurs according to the following reactions [16,17].

$$Sn^{4+} + OH^- \rightarrow Sn(OH)_4 \quad (1)$$

$$Sn(OH)_4 + 2OH^- \rightarrow [Sn(OH)_6]^{2-} \quad (2)$$

$$[Sn(OH)_6]^{2-} \rightarrow SnO_2 + 2H_2O + 2OH^- \quad (3)$$

Under alkali condition, Sn^{4+} reacts with OH^- to form small $Sn(OH)_4$ particles in Eq. (1), when OH^- is excessive, it can take place a chemical reaction (Eq. (2)), then $[Sn(OH)_6]^{2-}$ complex species are subsequently transformed into SnO_2 nanorods by a hydrothermal process according to Eq. (3).

Fig. 3 shows the FTIR spectra of graphite and SnO_2/graphite composite. For the natural flake graphite, the peak at 1584 cm^{-1} can be attributed to C=C bending vibrations [18]. The FTIR spectrum of SnO_2/graphite composite differs from that of graphite as evidenced by the appearing of the peaks at 3011, 1208 and 931 cm^{-1}. The peak at 3011 cm^{-1} and 1208 cm^{-1} are associated with stretching of the O–H band

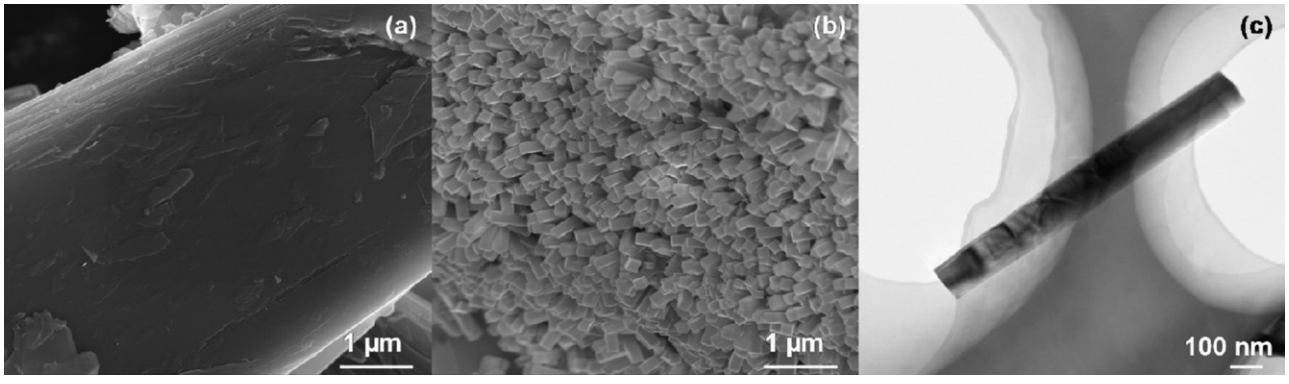

Fig. 2. (a) SEM pattern of graphite, (b) SEM pattern of SnO_2/graphite composite, (c) TEM pattern of single SnO_2 nanorod.

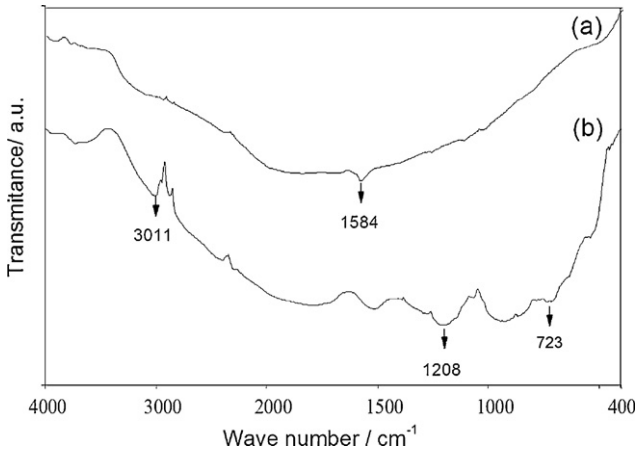

Fig. 3. FTIR spectra of (a) graphite, (b) SnO_2/grapite composite.

derived from NaOH. The peak at 723 cm^{-1} can be ascribed to lattice absorption of metallic oxide [19], indicating the strong adhesion between graphite and SnO_2 nanorods.

The N_2 adsorption/desorption isotherms of the as-prepared products are shown in Fig. 4. The SnO_2/graphite composite possesses 1.89 $m^2 g^{-1}$ of special surface area, between 1.3 $m^2 g^{-1}$ [19] (bare SnO_2) and 3.15 $m^2 g^{-1}$ (graphite). The total pore volumes of SnO_2/graphite composite, bare SnO_2 and graphite are about 0.01 $cm^3 g^{-1}$, 0.005 $cm^3 g^{-1}$ [19] and 0.017 $cm^3 g^{-1}$, respectively, indicating that graphite in composite could act as buffering spaces to hinder SnO_2 nanorods agglomeration.

The electrochemical properties of SnO_2 nanorods grown on graphite were investigated by galvanostatic charge/discharge, cyclic voltammetry measurements and electrochemical impedance spectroscopy. Fig. 5a shows the typical charge/discharge profiles of SnO_2/graphite composite at 1st, 2nd and 10th cycles at a current density of 50 mA g^{-1} in a voltage range from 0 to 3.0 V. In the first cycle, the SnO_2/graphite composite presents an obvious plateau at 0.95 V (vs. Li/Li^+) corresponds to the irreversible reduction of SnO_2 to form Li_2O and Sn [20]. The SnO_2/graphite composite delivers a lithium insertion capacity of 1197 mAh g^{-1} and a reversible charging capacity of 872 mAh g^{-1} with coulombic efficiency of 73%. The initial capacity loss may result from the incomplete conversion reaction and irreversible lithium loss due to the formation of a solid electrolyte interphase (SEI) layers [21,22]. From the second cycle, coulombic efficiency is improved significantly. After 10 cycles, the SnO_2/graphite composite still retains a reversible capacity of 627 mAh g^{-1}.

The electrochemical reactivity of SnO_2/graphite composite was evaluated by cyclic voltammetry (CV). Fig. 5b displays the CV curves of SnO_2/graphite composite in the first three scanning cycles at 0.2 mV s^{-1} in the range of 0–3.0 V. The behavior of the CV curves represents electrochemical reactions caused from both graphite and SnO_2 during cycling. In the first cycle, there is a strong cathodic peak around 0.75 V that occurs from the reduction of SnO_2 and the formation of a solid electrolyte interphase (SEI) layer [16]. The peak near 0 V is ascribed to Li intercalation into graphite to form LiC_6 [23]. The other reduction peaks are located between 0.75 V and 0 V, which can be ascribed to the formation of LixSn [24]. In the anodic curve, the peaks at 0.2 V and 0.5 V can be attributed to Li deintercalation from LiC_6 and Li dealloying from LixSn, respectively [16], while the weak oxidation peak at 1.23 V could be the partly reversible reaction from Sn to SnO_2 [25].

Cycle performances of SnO_2/graphite composite were further investigated at the current densities of 50 mA g^{-1}, 100 mA g^{-1} and 500 mA g^{-1} in Fig. 5c. The SnO_2/graphite composite exhibits superior cycle stability as compared to bare SnO_2. It has the advantages of both high capacity of SnO_2 and superior conductivity of graphite. After 40 cycles at different current densities, it was found that the reversible discharge capacity of SnO_2/graphite composite was still maintained at 408 mAh g^{-1}, much higher than that of graphite and bare SnO_2.

In Fig. 5d, the EIS spectra are combinations of a semicircle in high frequencies and a straight line in low frequencies. Interpretation of the impedance spectra is based on the equivalent circuit on the left. The symbols Rs, Rct, Cd, and Zw represent the solution resistance, charge-transfer resistance, capacitance of the double layer, and Warburg impedance, respectively [26]. In the high-frequency region, the intercept

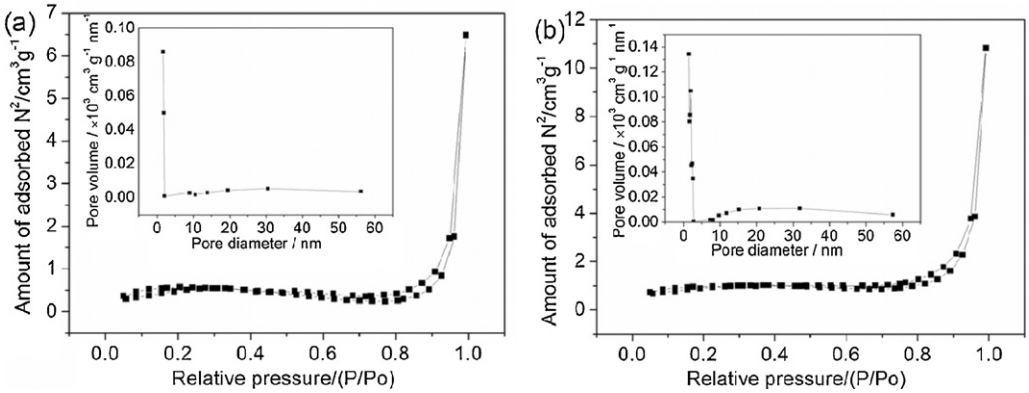

Fig. 4. Nitrogen adsorption/desorption isotherms of (a) SnO_2/graphite composite, (b) graphite, inset shows the porosity distribution by Original Density Functional Theory Model.

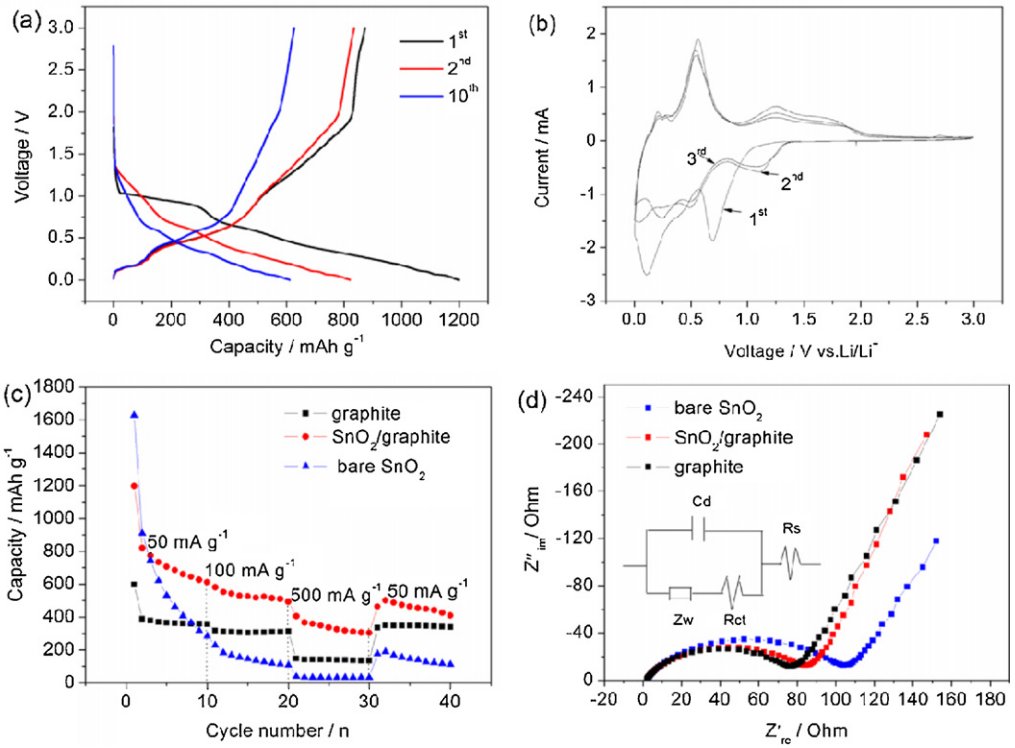

Fig. 5. (a) Charge/discharge profiles of SnO_2/graphite composite at current density of 50 mA g^{-1}, (b) cyclic voltammograms of SnO_2/graphite composite at a scanning rate of 0.2 mV s^{-1}, (c) cycle performances of SnO_2/graphite composite, graphite and bare SnO_2 at various current densities, (d) EIS spectra of the fresh SnO_2/graphite composite electrode in three-electrode configuration in 1 M $LiPF_6$/EMC-DEC (1:1, v/v) at 20 °C in the frequency range from 0.1 to 100 kHz.

with real impedance [Re(Z)] axis of SnO_2/graphite composite is 83 Ω, between 76 Ω (graphite) and 104 Ω (bare SnO_2), which is believed to be the total electronic resistance of the electrode materials. In the low frequency region, the faradaic reaction is the main effect. The slope of the impedance of SnO_2/graphite composite is bigger than that of graphite and bare SnO_2, indicating that the superior Li^+ diffusion speed of SnO_2/graphite composite.

4. Conclusions

In summary, we have developed a facile strategy to synthesize a novel architecture of SnO_2 nanorods grown on graphite surface. Rectangular-shaped SnO_2 nanorods are highly crystalline with a tetragonal rutile phase and distribute uniformly on the surface of natural flake graphite. The SnO_2/graphite composite exhibits an enhanced reversible lithium storage capacity and good cyclic performance as anode material for lithium-ion batteries.

References

[1] J.A. Choi, K.S.H. Kim, D.W. Kim, Enhancement of thermal stability and cycling performance in lithium-ion cells through the use of ceramic-coated separators, J. Power Sources 195 (18) (2010).
[2] Y. Kumai, S. Shirai, E. Sudo, J. Seki, H. Okamoto, Y. Sugiyama, H. Nakano, Characteristics and structural change of layered polysilane (Si_6H_6) anode for lithium ion batteries, J. Power Sources 196 (3) (2011) 1503–1507.
[3] Y. Li, B. Tan, Y. Wu, Mesoporous Co_3O_4 nanowire arrays for lithium ion batteries with high capacity and rate capability, Nano Lett. 8 (1) (2008) 265–270.
[4] C. Yong, L. Shuang, Y. Xiaoming, H. Quanyi, Z. Ming, W. Taihong, Facile preparation of porous one-dimensional Mn_2O_3 nanostructures and their application as anode materials for lithium-ion batteries, Physica E 43 (1) (2010).
[5] Z.M. Cui, L.Y. Hang, W.G. Song, Y.G. Guo, High-yield gas–liquid interfacial synthesis of highly dispersed Fe_3O_4 nanocrystals and their application in lithium-ion batteries, Chem. Mater. 21 (6) (2009) 1162–1166.
[6] X.H. Huang, X.H. Xia, Y.F. Yuan, F. Zhou, Porous ZnO nanosheets grown on copper substrates as anodes for lithium ion batteries, Electrochim. Acta 56 (14) (2011) 4960–4965.
[7] L.M. Li, X.M. Yin, S.A. Liu, Y.G. Wang, L.B. Chen, T.H. Wang, Electrospun porous SnO_2 nanotubes as high capacity anode materials for lithium ion batteries, Electrochem. Commun. 12 (10) (2010) 1383–1386.
[8] M. Pfanzelt, P. Kubiak, M. Fleischhammer, M. Wohlfahrt-Mehrens, TiO_2 rutile—an alternative anode material for safe lithium-ion batteries, J. Power Sources 196 (16) (2011) 6815–6821.
[9] P. Guo, H. Song, X. Chen, Electrochemical performance of graphene nanosheets as anode material for lithium-ion batteries, Electrochem. Commun. 11 (6) (2009) 1320–1324.
[10] X.Y. Wang, X.F. Zhou, K. Yao, J.G. Zhang, Z.P. Liu, A SnO_2/graphene composite as a high stability electrode for lithium ion batteries, Carbon 49 (1) (2011) 133–139.
[11] Z.S. Wu, W. Ren, L. Wen, L. Gao, J. Zhao, Z. Chen, G. Zhou, F. Li, H.-M. Cheng, Graphene anchored with Co_3O_4 nanoparticles as anode of lithium ion batteries with enhanced reversible capacity and cyclic performance, Acs Nano 4 (6) (2010) 3187–3194.
[12] L. Xing, C. Cui, C. Ma, X. Xue, Facile synthesis of alpha-MnO_2/graphene nanocomposites and their high performance as lithium-ion battery anode, Mater. Lett. 65 (14) (2011) 2104–2106.
[13] G. Zhou, D.W. Wang, F. Li, L. Zhang, N. Li, Z.S. Wu, L. Wen, G.Q. Lu, H.M. Cheng, Graphene-wrapped Fe_3O_4 anode material with improved reversible capacity and cyclic stability for lithium ion batteries, Chem. Mater. 22 (18) (2010) 5306–5313.

[14] F. Wang, G. Yao, M. Xu, M. Zhao, Z. Sun, X. Song, Large-scale synthesis of macroporous SnO_2 with/without carbon and their application as anode materials for lithium-ion batteries, J. Alloys Compd. 509 (20) (2011) 5969–5973.

[15] P. Wu, N. Du, H. Zhang, J.X. Yu, Y. Qi, D.R. Yang, Carbon-coated SnO_2 nanotubes: template-engaged synthesis and their application in lithium-ion batteries, Nanoscale 3 (2) (2011) 746–750.

[16] J.G. Kim, S.H. Nam, S.H. Lee, S.M. Choi, W.B. Kim, SnO_2 nanorod-planted graphite: an effective nanostructure configuration for reversible lithium ion storage, Acs Appl. Mater. Int. 3 (3) (2011) 828–835.

[17] Y. Han, X. Wu, G. Shen, B. Dierre, L. Gong, F. Qu, Y. Bando, T. Sekiguchi, F. Filippo, D. Golberg, Solution growth and cathodoluminescence of novel SnO_2 core–shell homogeneous microspheres, J. Phys. Chem. C 114 (18) (2010) 8235–8240.

[18] J. Shen, Y. Hu, M. Shi, N. Li, H. Ma, M. Ye, One step synthesis of graphene oxide-magnetic nanoparticle composite, J. Phys. Chem. C 114 (3) (2010) 1498–1503.

[19] H.D. Liu, J.H. Huang, X.L. Li, J. Liu, Y.X. Zhang, K. Du, Flower-like SnO_2/graphene composite for high-capacity lithium storage, Appl. Surf. Sci. 258 (11) (2012) 4917–4921.

[20] R. Yang, Y. Gu, Y. Li, J. Zheng, X. Li, Self-assembled 3-D flower-shaped SnO_2 nanostructures with improved electrochemical performance for lithium storage, Acta Mater. 58 (3) (2010) 866–874.

[21] C. Wang, Y. Zhou, M.Y. Ge, X.B. Xu, Z.L. Zhang, J.Z. Jiang, Large-scale synthesis of SnO_2 nanosheets with high lithium storage capacity, J. Am. Chem. Soc. 132 (1) (2010) 46–47.

[22] X.W. Lou, D. Deng, J.Y. Lee, L.A. Archer, Preparation of SnO_2/carbon composite hollow spheres and their lithium storage properties, Chem. Mater. 20 (20) (2008) 6562–6566.

[23] P. Lian, X. Zhu, S. Liang, Z. Li, W. Yang, H. Wang, Large reversible capacity of high quality graphene sheets as an anode material for lithium-ion batteries, Electrochim. Acta 55 (12) (2010) 3909–3914.

[24] P.C. Lian, X.F. Zhu, S.Z. Liang, Z. Li, W.S. Yang, H.H. Wang, High reversible capacity of SnO_2/graphene nanocomposite as an anode material for lithium-ion batteries, Electrochim. Acta 56 (12) (2011) 4532–4539.

[25] J. Yao, X. Shen, B. Wang, H. Liu, G. Wang, In situ chemical synthesis of SnO_2-graphene nanocomposite as anode materials for lithium-ion batteries, Electrochem. Commun. 11 (10) (2009) 1849–1852.

[26] X. Li, S.H. Yoon, K. Du, Y. Zhang, J. Huang, F. Kang, An urchin-like graphite-based anode material for lithium ion batteries, Electrochim. Acta 55 (19) (2010) 5519–5522.